

Modeling segregation of bidisperse granular materials using physical control parameters in the quasi-2D bounded heap

Conor P. Schlick,^{1, a)} Yi Fan,^{2, 3} Austin B. Isner,⁴ Paul B. Umbanhowar,² Julio M. Ottino,^{2, 4, 5} and Richard M. Lueptow^{2, 5, b)}

¹⁾ *Department of Engineering Sciences and Applied Mathematics, Northwestern University, Evanston, IL 60208, USA*

²⁾ *Department of Mechanical Engineering, Northwestern University, Evanston, IL 60208, USA*

³⁾ *The Dow Chemical Company, Midland, MI 48667, USA*

⁴⁾ *Department of Chemical and Biological Engineering, Northwestern University, Evanston, IL 60208, USA*

⁵⁾ *The Northwestern Institute on Complex Systems (NICO), Northwestern University, Evanston, IL 60208, USA*

(Dated: 31 October 2014)

Quantitatively predicting segregation patterns of size-disperse granular materials is of potential value in many industrial applications. We consider granular segregation of size-bidisperse particles in quasi-2D bounded heaps, a canonical granular flow, using an advection-diffusion transport equation with an additional term to account for particle segregation. The equation is characterized by two dimensionless parameters that are functions of control parameters (flow rate, system size, and particle sizes) and kinematic parameters (flowing layer depth, diffusion coefficient, and percolation length scale). As the kinematic parameters are usually difficult to measure in practice, their dependence on the control parameters is determined directly from discrete element method (DEM) simulations. Using these relationships, it is possible to determine which values of the control parameters result in a mixed or segregated heap. The approach used here is broadly applicable to a wide range of other flow geometries and particle systems.

I. INTRODUCTION AND BACKGROUND

Segregation of granular materials composed of different sizes occurs in many industrial situations, but is difficult to predict. Several studies have focused on understanding size segregation of sheared granular flows in chutes, silos, tumblers, and heaps.^{1–7} In dense granular flows, a percolation mechanism^{3, 8–10} has been proposed: small particles fall downward through shear-generated voids under gravity, and large particles thus move upward. Percolation, along with advection due to a mean flow and diffusion due to random particle collisions, have been shown to produce complex segregation patterns.^{5, 6, 11, 12}

A recent model can predict whether segregation or mixing will occur for bidisperse particles in quasi-two-dimensional bounded heap flow.¹³ The model, explained in detail in section IB, is characterized by two dimensionless parameters that depend on dimensional control parameters (e.g. flow rate, system size, and particle sizes) and kinematic parameters (e.g. diffusion coefficient, flowing layer depth, and percolation length scale), which can be obtained from discrete element method (DEM) simulations.¹⁴ In this paper, we determine the relationships between the control parameters and the kinematic parameters, so that the dimensionless parameters can be estimated based on the control parameters only, allowing the theoretical model to be implemented without

the need for detailed DEM simulations specific to the flow conditions. With this knowledge, we parametrically study mixing and segregation of size bidisperse particles in quasi-two-dimensional (quasi-2D) bounded heaps in terms of the control parameters, and provide a general relation for the percolation length scale of the large and small particles as a function of the particle size ratio.

A. Quasi-two-dimensional bounded heap flow

As an example of a system in which to apply the transport equation approach, we consider segregation of bidisperse particles in quasi-2D bounded heap flow, shown schematically in figure 1(a). Quasi-2D bounded heap flow occurs in numerous industrial filling operations of narrow cuboidal containers, which can range in size from consumer laundry and cereal boxes to train cars and shipping containers. Moreover, it provides a relatively well-characterized system to test relations associated with the model. In our realization of quasi-2D bounded heap flow, granular material is fed by gravity at the left end of the container at a mass flow rate \dot{m} . Grains fall and form a heap (with a dynamic angle of repose, α), which eventually extends to the right end wall. For steady filling (no avalanching^{6, 15}), the free surface of the heap rises with uniform velocity $v_r = \dot{m}/(\rho fWT)$, where ρ is the particle density, f is the solids fraction, and T and W are the thickness and width of the container, respectively. In this study, we focus on containers that are 4-6 large particle diameters thick, although the approach can readily be

^{a)} Electronic mail: conorschlick2015@u.northwestern.edu

^{b)} Electronic mail: r-lueptow@northwestern.edu

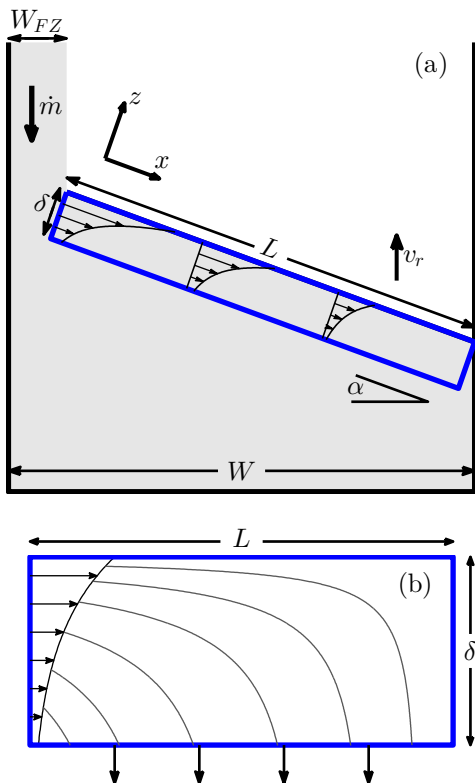


FIG. 1. (a) Schematic of quasi-2D bounded heap flow. Particles are dropped onto the heap at mass flow rate \dot{m} on the left, and the heap rises with rise velocity v_r . The domain has width W and thickness T . Particles flow down and to the right in a thin flowing layer (grey box, blue online) of length L and thickness δ and are deposited continuously at various streamwise locations in the solid bed. The coordinate system is rotated by the angle of repose, α , such that the x -coordinate is in the streamwise direction, the y -coordinate is in the spanwise direction, and the z -coordinate is normal to the free surface. The origin is located at the top left corner of the flowing layer and rises with the heap. (b) Close-up of the flowing layer in the moving reference frame, showing streamlines for the mean flow of particles and streamwise velocity profile at $x = 0$. The flowing layer thickness, δ , which is typically $O(10)$ particles thick, is exaggerated in size relative to the flowing layer length.

applied to different thicknesses. Almost all motion takes place in a thin flowing layer of length L and depth δ near the free surface (rectangle in figure 1(a)). A close-up of the flowing layer with streamlines in the moving reference frame is shown in figure 1(b). Particles enter the left side of the flowing layer and are deposited from the bottom of the flowing layer onto the solid bed continuously along the length of the heap. Note that figure 1(a) could also represent one side of a two-sided heap if the left wall were replaced by a line of symmetry.

Here we consider an initially mixed size bidisperse mixture that enters the flowing layer on the left end. Small particles percolate through shear-generated voids, fall to the bottom of the flowing layer, and are deposited on

the heap upstream. Conversely, large particles rise to the top of the flowing layer and are advected further downstream before being deposited on the heap. Consequently, small and large particles are separated in the streamwise direction.^{6,8,9,16–18}

Several models of size segregation in bounded heap flow have been previously proposed.^{17,19–21} The primary shortcoming of these models is that they depend on either arbitrarily adjustable fitting parameters that do not have a clear physical interpretation^{17,19} or “collision functions,” which are *a priori* unknown.^{20,21} Without knowing these parameters or functions, it is difficult to predict final segregation patterns based on only the system control parameters. In contrast to these studies, Fan *et al.*¹³ were able to quantitatively predict experimental segregation patterns based on control parameters and kinematic parameters, which are measured from DEM simulations, that have clear physical meaning. In this work, we develop the scaling relations between the kinematic parameters (e.g. segregation length scale, flowing layer depth, and diffusion coefficient) and the control parameters, eliminating the need for DEM simulations. More importantly, the functional relations developed here can be readily applied to other granular flow geometries such as rotating tumblers.²²

To validate the theoretical model, we compare our predictions to experimental measurements of quasi-2D bounded heaps from Fan *et al.*,⁶ see figure 2(a) for an image of the experimental apparatus and a typical segregation pattern. The quasi-2D bounded heap is formed between two glass plates, and particles are dropped onto the left side of the heap using a screw feeder. The white lines indicate the steady filling region of the heap that we model here. Since the theoretical model¹³ requires detailed knowledge of the velocity field, we also use DEM simulations, shown in figure 2(b) and explained in more detail in section II A. DEM simulations allow us to determine the kinematic parameters for many different flow rates and particle sizes, making it possible to develop scaling relations between the kinematic parameters and the control parameters. The concentration profiles of the experiment and the DEM simulation are quantitatively similar,²³ with the small particles deposited in the upstream (left) portion of the heap, and the large particles in the downstream (right) portion of the heap.

B. Theoretical model

The effects of percolation can be combined with advection due to mean flow and diffusion due to random particle collisions through the scalar transport equation. Versions of this continuum (Eulerian) approach have been applied to plug,^{24–26} chute,^{27–31} and annular shear³² flows, and qualitative agreement between theory, experiments, and simulations has been shown. However, these studies have not achieved quantitative agreement, possibly due to oversimplifying the flow kinematics, neglecting

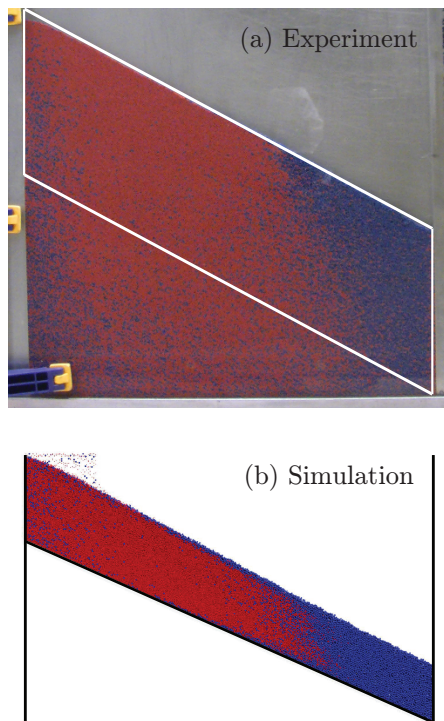


FIG. 2. (a) Experimental image⁶ and (b) DEM simulation image of a quasi-2D bounded heap of 1 mm (grey, red online) and 2 mm (black, blue online) glass spheres. Well mixed particles are fed by gravity at the left side of the heap. The white lines in (a) indicate the steady filling domain of the heap in the experiment. For the DEM simulation, the bottom wall is inclined so that fewer particles need to be simulated in the steady-filling domain, which decreases computational time. $\dot{m} = 18.4$ g/sec, $W = 0.44$ m, and $T = 9$ mm.

diffusion, or omitting the dependence of the percolation velocity on the spatially varying shear rate.⁹ Our recent study¹³ achieved quantitative agreement between theory, experiments, and simulations using this transport equation approach. In this approach, the transport equation

$$\frac{\partial c_i}{\partial t} + \nabla \cdot (\mathbf{u}c_i) + \frac{\partial}{\partial z}(w_{p,i}c_i) = \nabla \cdot (D\nabla c_i), \quad (1)$$

$$x \in [0, L], \quad z \in [-\delta, 0],$$

is applied to the flowing layer ($0 < x < L$, $-\delta < z < 0$), since this is where segregation occurs. In bidisperse mixtures, i refers to the small or large particles (i.e. $i = s$ or $i = l$), and no subscript is used for variables representing the combined flow. The concentration of species i is given as $c_i = f_i/f$, where f_i is the volume fraction of species i and $f = f_s + f_l$, which is approximately constant for bounded heaps.²³ $\mathbf{u} = u\hat{x} + v\hat{y} + w\hat{z}$ is the mean velocity field of both species, D is the diffusion coefficient, and $w_{p,i}$ is the percolation velocity of species i , which accounts for the relative motion of the two species in the normal direction.

To solve equation (1), the mean velocity field \mathbf{u} , the percolation velocity $w_{p,i}$, the diffusion coefficient D , and

the flowing layer depth δ must be known. Using DEM simulations, these quantities can be calculated across a broad range of the control parameters (particle sizes, flow rates, and lengths of the flowing layer). It has been previously shown that the percolation velocity is a linear function of the shear rate¹³ and the concentration of the other species:^{10,13}

$$w_{p,i} = S\dot{\gamma}(1 - c_i), \quad (2)$$

where $\dot{\gamma} = \frac{\partial u}{\partial z}$ and S is the signed percolation length scale (positive for large particles, negative for small particles), and is determined from DEM simulations. This relation is validated in section II B.

Equation (1) is nondimensionalized using:

$$\tilde{x} = \frac{x}{L}, \quad \tilde{z} = \frac{z}{\delta}, \quad \tilde{t} = \frac{t}{\delta L/2q},$$

$$\tilde{u} = \frac{u}{2q/\delta}, \quad \text{and} \quad \tilde{w} = \frac{w}{2q/L}, \quad (3)$$

where q is the 2D flow rate defined as

$$q = v_r L \cos(\alpha) = \frac{\dot{m}L \cos(\alpha)}{\rho f T W}. \quad (4)$$

Averaging over the spanwise (y) direction, neglecting diffusion in the streamwise (x) direction (which is valid if $\delta/L \ll 1$), and substituting this set of nondimensional quantities into equation (1) yields

$$\frac{\partial c_i}{\partial \tilde{t}} + \tilde{u} \frac{\partial c_i}{\partial \tilde{x}} + \tilde{w} \frac{\partial c_i}{\partial \tilde{z}} \pm \Lambda \frac{\partial}{\partial \tilde{z}} [h(\tilde{x}, \tilde{z})c_i(1 - c_i)]$$

$$= \frac{\partial}{\partial \tilde{z}} \left(\frac{1}{\text{Pe}} \frac{\partial c_i}{\partial \tilde{z}} \right), \quad (5)$$

where the “+” sign is taken for large particles and the “−” sign is taken for small particles. The two dimensionless parameters are $\Lambda = |S|L/\delta^2$ and $\text{Pe} = 2q\delta/DL$, and $h(\tilde{x}, \tilde{z}) = \dot{\gamma}\delta^2/2q$ is the dimensionless shear rate. The numerical method used to solve this equation (with appropriate boundary conditions) is described in appendix A.

Λ and Pe are functions of the control parameters (q , L , d_s , and d_l), where d_s and d_l are the diameters of the small and large particles, and the kinematic parameters (D , δ , and $|S|$). Λ is the ratio of an advection time scale ($L/u = \delta/w = L\delta/2q$) to a segregation time scale ($\delta/w_p = \delta^3/2|S|q$), and Pe , the Péclet number, is the ratio of a diffusion timescale (δ^2/D) to an advection timescale ($L/u = \delta/w = L\delta/2q$). Given the velocity field \tilde{u} and \tilde{w} and the corresponding dimensionless shear rate $h(\tilde{x}, \tilde{z})$, the final particle configuration is solely a function of Λ and Pe .

C. Motivation

Implementation of the theoretical model for bounded heaps requires the specification of $\Lambda = |S|L/\delta^2$ and Pe

$= 2q\delta/LD$. These two parameters are related to both the control parameters and the kinematic parameters. While the control parameters are specified directly, the kinematic parameters must be extracted from DEM simulations, which can be quite costly. Thus, without knowing the relation between the kinematic parameters and the control parameters, it is difficult to apply the model across a wide range of flow conditions without running extensive DEM simulations.

In section II of this paper, we first use DEM simulations to determine the kinematic parameters for a wide range of control parameters in order to establish general relations between the parameters. This allows the implementation of the theoretical model¹³ without DEM simulations. In section III, we parametrically study the segregation states of bidisperse mixtures in quasi-2D bounded heap flow in terms of the control parameters, determining which conditions result in a mixed state and which result in a segregated state.

II. SCALING OF KINEMATIC PARAMETERS

DEM simulations were performed at numerous flow rates and with different particle sizes to establish the relations between kinematic and control parameters.

A. Discrete element method simulations

DEM simulations like that shown in figure 2(b) are based on tracking the translational and rotational momenta of each particle via integration of Newton's equation of motion. Spherical glass particles are modeled as "soft" inelastic spheres through the use of a contact-only repulsive normal force, as in our previous work.^{13,23} Particles in the simulation have a material density $\rho = 2500 \text{ kg/m}^3$ and a restitution coefficient $\varepsilon = 0.8$. Particle-particle and particle-wall friction coefficients, μ , are 0.4. These values reflect those for spherical glass particles and have been confirmed in Fan *et al.*²³ To decrease computational time, the binary collision time is set to $t_c = 10^{-3} \text{ s}$, consistent with previous simulations^{23,33} and sufficient for modeling hard spheres.³⁴ The integration time step is $t_c/40 = 2.5 \times 10^{-5} \text{ s}$ to assure numerical stability.

As described in Fan *et al.*,¹³ the bottom bounding wall of the quasi-2D heap is inclined at an angle of 24° , similar to the dynamic angle of repose α measured from experiments. In this way, the steady-filling regime is achieved much faster and with fewer particles necessary to form the base of the heap. The heap width was kept approximately constant for all simulations, at $W \approx 0.44 \text{ m}$. The gap thickness, T , was kept between 4 and 6 large particle diameters thick (i.e. $4d_l \leq T \leq 6d_l$). In all simulations, particles fall onto the left end of the heap in a 8 cm wide feed zone from a height of approximately 10 cm above the bottom wall.

Unlike our previous work,^{13,23} the DEM simulations were performed using a parallelized algorithm on a Nvidia GTX 780 graphics card (Graphics Processing Unit, or GPU) installed on a desktop computer running Ubuntu Linux 12.04LTS. A custom-developed code written in the Nvidia CUDA programming language was used to implement the DEM simulations. The GPU-based framework for DEM simulations allowed us to achieve the much greater number of simulations needed to determine the relationships between the kinematic parameters and the control parameters within a reasonable amount of time. For example, a simulation of quasi-2D bounded heaps with 10^5 particles takes approximately 8-10 hours to complete using the Nvidia GTX 780 graphics card compared to 3 days using a traditional serial algorithm on a dual-socket Intel Xeon 5690 processor (used in our previous work).^{13,23} Consequently, a total of 110 DEM simulations of varying particle size ratios and feed rates were performed. The DEM simulations were validated by comparing concentration profiles from experiments and flow kinematics from previously validated numerical simulations.

B. Mean velocities and percolation velocity

We assume that the streamwise velocity profile, u , is the same for large and small particles.³⁵ The DEM simulations are consistent with the theoretical prediction for a uniformly rising flat flowing layer in that the surface velocity $u(x, 0)$ decreases approximately linearly with the streamwise position x , as shown in figure 3(a). The streamwise velocity u decreases with depth in the flowing layer as shown in figure 3(b). An exponential form for the streamwise velocity profiles works reasonably well for predicting segregation patterns.¹³ Combining these two results yields

$$u(x, z) = \frac{kq}{\delta(1 - e^{-k})} \left(1 - \frac{x}{L}\right) e^{kz/\delta}. \quad (6)$$

k is set equal to 2.3 so that the streamwise velocity at the bottom of the flowing layer, $z = -\delta$, is 10% of the surface velocity (i.e. $\exp(-2.3) \approx 0.1$).³⁶ Using continuity along with the boundary condition $w(x, 0) = 0$ yields the mean normal velocity:

$$w(x, z) = \frac{q}{L(1 - e^{-k})} \left(e^{kz/\delta} - 1\right). \quad (7)$$

The normal velocity for each particle species, however, depends on both the mean velocity of both particle species together and a velocity representing the percolation of each species. Therefore, $w_i = w + w_{p,i}$ where w_i is the normal velocity of species i , w is the mean normal velocity, and $w_{p,i}$ is the percolation velocity of species i . In sheared granular flows, small particles percolate downward between shear-generated particle voids, and the large particles rise up, so $w_{p,s} < 0$ and $w_{p,l} > 0$.

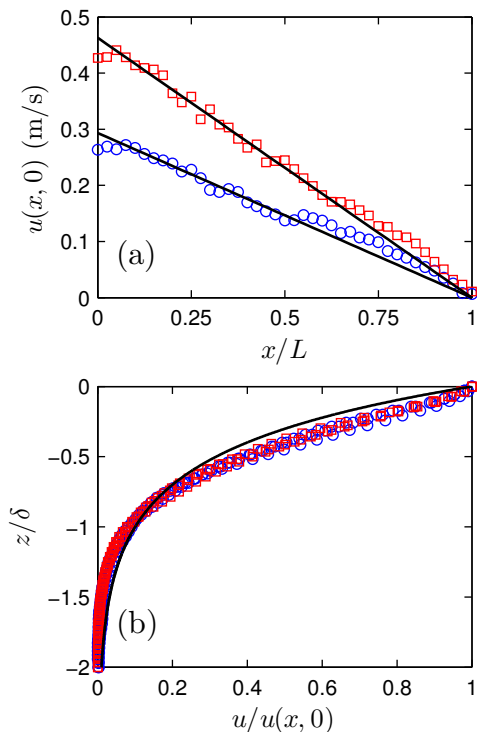


FIG. 3. (a) Surface velocity $u(x,0)$ vs. x and (b) the streamwise velocity profile, u , normalized by the surface velocity ($u(x,z)/u(x,0)$) at different streamwise locations. $q = 4.20 \times 10^{-3} \text{ m}^2/\text{s}$, $d_s = 1.75 \text{ mm}$, $d_l = 3 \text{ mm}$, $L = 0.40 \text{ m}$ (\square); $q = 3.30 \times 10^{-3} \text{ m}^2/\text{s}$, $d_s = 3 \text{ mm}$, $d_l = 4 \text{ mm}$, $L = 0.40 \text{ m}$ (\circ). Line in (a) and curve in (b) are from equation (6) (i.e. $u(x,0) \sim (1 - x/L)$ and $u/u(x,0) = \exp(kz/\delta)$, respectively).

The percolation velocity depends on the local volume concentration of each species, since the void sizes are associated with the local packing. For example, percolation of a small particle is enhanced when more large particles surround it. Savage and Lun found¹⁰ that, in sheared flows of bidisperse mixtures, the percolation velocity of each species is proportional to the concentration of the other species, $w_{p,i} \sim (1 - c_i)$, as well as the shear rate. This relation has been used in other studies.^{24,37,38} Equation (2) for the percolation velocity also defines a constant of proportionality, S , which is the signed percolation length scale. Accordingly, the local percolation velocity, $w_{p,i}$, and the volume concentration, c_i , of each species are measured from DEM simulations to investigate the dependence of S on the particle size ratio in bounded heap flow. Figure 4 shows an example of the percolation velocity of each species as a function of the local concentration of the other species for 1.25 and 2.25 mm diameter particles at $q = 4.02 \times 10^{-3} \text{ m}^2/\text{s}$ in the flowing layer (over 500 data points are included spanning the entire length and depth of the flowing layer).³⁹ To collapse the data in figure 4, the local percolation velocity is divided by the local shear rate, $\dot{\gamma} = \partial u/\partial z$. The data over the entire length and depth of the flowing layer

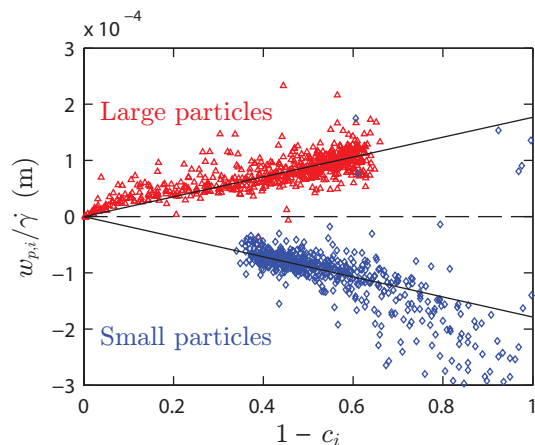


FIG. 4. Dependence of percolation velocity on particle concentrations and shear rate. $w_{p,i}/\dot{\gamma}$ vs. $(1 - c_i)$ for large (gray, red online, Δ) and small (black, blue online, \diamond) particles. Solid lines are a linear fit of the data, yielding $S_s = -0.1787 \text{ mm}$ and $S_l = 0.1768 \text{ mm}$. $q = 4.02 \times 10^{-3} \text{ m}^2/\text{s}$, $d_s = 1.25 \text{ mm}$, $d_l = 2.25 \text{ mm}$, $L = 0.41 \text{ m}$.

collapse well and can be approximated by equation (2), where S is the slope of the linear fit of the i^{th} particle species percolation velocity data. For example, figure 4 shows the linear fits to percolation velocities for the large and small particles from a single DEM simulation.

In the model, we assume that the magnitudes of S for the larger particles, S_l , and S for the smaller particles, S_s , are equal as required by mass conservation if the solids fraction remains constant (i.e. $\nabla f = \mathbf{0}$). For the particular case shown in figure 4, $|S_s| = 0.179 \text{ mm}$ and $S_l = 0.177 \text{ mm}$, which is typical of the similarity in magnitude between S_s and S_l for the DEM simulations. The average magnitude of S is computed as $|S| = (|S_s| + |S_l|)/2$, which we define to be the percolation length scale. S depends on both the particle size ratio, $R = d_i/d_j$, and the absolute particle sizes.¹³ Data for $1 - c_s > 0.9$ were neglected when fitting a line to the data in figure 4 because equation (2) no longer accurately describes the percolation velocity (see figure 4). However, this region only occurs at the right end of the heap where the number of large particles dominates the number of small particles. Consequently, using equation (2) in this region has no effect on the theoretical predictions in most of the flowing layer. Equation (2) necessarily satisfies mass conservation because the total net flux, $c_s w_{p,s} + c_l w_{p,l}$, is zero (since $c_s = 1 - c_l$).

The approach used in figure 4 is repeated over a broad range of particle sizes and size ratios to determine S as a function of the two particle sizes. Since S was shown to be insensitive to q ,¹³ only one flow rate ($\dot{m} = 90 \text{ g/s}$) was used for the simulations. In figure 5, S for larger particles is plotted versus $R = d_l/d_s > 1$, and S for smaller particles is plotted versus $R = d_s/d_l < 1$. Each d_i/d_j pair ($R = d_l/d_s$ for S_l and $R = d_s/d_l$ for S_s) represents one DEM simulation, where $1 \text{ mm} \leq d_i, d_j \leq$

4 mm. For $1/3 < R < 3$, S normalized by d_s is an approximately linear function of $\log(R)$:

$$\frac{S}{d_s} = C_S \log R, \quad (8)$$

where $C_S = 0.26$. This relation for the percolation length scale, along with figure 5, is a key result of this paper. While equation (8) was derived for quasi-2D bounded heap flow, it may be possible to apply this to other granular systems, including rotating tumblers.²²

Outside the range $1/3 < R < 3$ ($3 \leq R \leq 4$ and $1/4 \leq R \leq 1/3$), S/d_s is approximately independent of R . A similar trend was also observed in experiments,⁴⁰ where it was found that the time for particles to segregate reached a minimum around $R \approx 2$. This is most likely due to “free-sifting” that occurs for larger R , in which small particles percolate downwards without significantly affecting the flow of large particles, particularly in a dilated bed of particles during flow. Another possible reason for the flattening of the curve is that, for large size ratios, the binary collision time, t_c , could be somewhat different for the large and small particles^{41–43} ($t_c = 10^{-3}$ s for all particles in our simulations), perhaps introducing some error into the simulations. Therefore, we limit R in the remainder of this paper to the range $1/3 < R < 3$. Note also that equation (8) is valid for spherical glass particles with density $\rho = 2500$ kg/m³; substantially more work remains to be done to determine the dependence of S on particle shape, density, and friction.

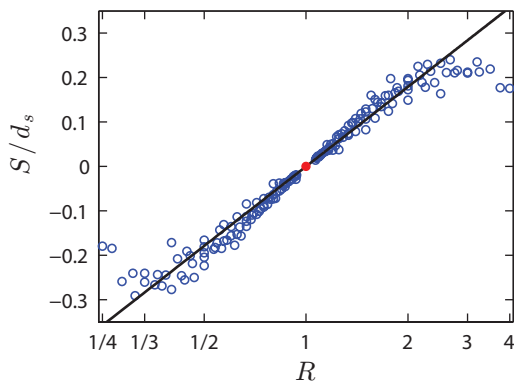


FIG. 5. S vs. $R = d_i/d_j$ for $1 \text{ mm} \leq d_i, d_j \leq 4 \text{ mm}$. Each pair of data points ($R = d_i/d_s > 1$ and $R = d_s/d_i < 1$) represents a single DEM simulation with $\dot{m} = 90$ g/s. The line is a fit of the data to equation (8) (where $C_S = 0.26$) for $1/3 < R < 3$. The dot (light gray, red online) at $R = 1$ ($d_i = d_j$) represents a monodisperse system ($S = 0$).

C. Flowing layer depth and diffusion coefficient

The bottom of the flowing layer is defined to be the depth where the streamwise velocity, u , is 10% of the sur-

face velocity, as in a previous study.²³ In the DEM simulations, the flowing layer depth is approximately constant in the upstream region ($x/L \lesssim 0.5$) and decreases slightly in the downstream region ($x/L \gtrsim 0.5$).²³ To simplify the modeling, δ is assumed to be constant along the entire flowing layer. The value for δ that is used is the maximum flowing layer depth in the streamwise direction, which occurs in the upstream region of the heap. This choice of δ is reasonable since the majority of the segregation occurs in this upstream region.

In figure 6(a), δ , normalized by the mean particle diameter $\bar{d} = (d_s + d_l)/2$, is plotted as a function of q , normalized by $\sqrt{g\bar{d}^3}$, similar to the scalings used previously.²³ Data for six different particle size mixtures collapses reasonably well, yielding the relation

$$\delta = C_\delta \bar{d} \left(\frac{q}{\sqrt{g\bar{d}^3}} \right)^{\beta_\delta}, \quad (9)$$

where $C_\delta = 4.10$ and $\beta_\delta = 0.35$.

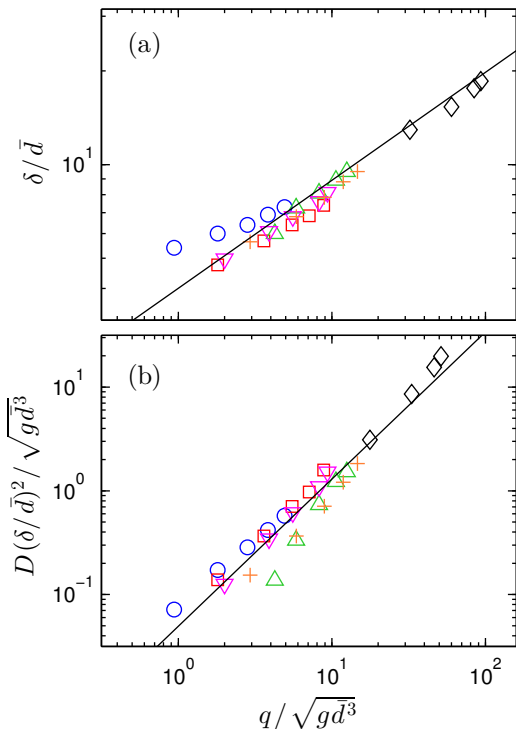


FIG. 6. (a) δ vs. q and (b) D vs. q for various particle sizes. For each data point, a DEM simulation was performed and the maximum value of δ and the average value of D in the flowing layer was calculated. $d_s = 2$ mm, $d_l = 4$ mm (\circ); $d_s = 1$ mm, $d_l = 3$ mm (\square); $d_s = 2$ mm, $d_l = 3$ mm (\triangle); $d_s = 1.5$ mm, $d_l = 3$ mm (∇); $d_s = 2$ mm, $d_l = 2$ mm ($+$); $d_s = 0.5$ mm, $d_l = 1$ mm (\diamond). Lines in (a) and (b) represent fits of the data to equations (9) and (10), respectively.

Finally, to determine the dependence of the diffusion coefficient D on the control parameters, the mean squared displacement from the average velocity of each

individual species in the DEM simulations was calculated. Previous work¹³ showed $D \sim \dot{\gamma}$ for dense granular flows of monodisperse^{44–47} and bidisperse^{13,48} particles. However, a constant value for D works well in the model.¹³ Hence, for simplicity, a value of D averaged across the entire flowing layer is extracted from the DEM simulations.

In figure 6(b), D , normalized by $\sqrt{g\bar{d}^3}(\bar{d}/\delta)^2$, is plotted as a function of q , normalized by $\sqrt{g\bar{d}^3}$. Again the data for the six different particle mixtures collapses reasonably well, yielding the relation

$$D = C_D \sqrt{g\bar{d}^3} \left(\frac{\bar{d}}{\delta} \right)^2 \left[\frac{q}{\sqrt{g\bar{d}^3}} \right]^{\beta_D}, \quad (10)$$

where $C_D = 0.055$ and $\beta_D = 1.42$. The scaling used for D may, at first glance, seem somewhat arbitrary. However, previous studies^{13,44,47,48} have shown that $D \sim \dot{\gamma}\bar{d}^2$ for rapid dense granular flow. From equation (6), $\dot{\gamma} = \partial u/\partial z \sim q/\delta^2$. Combining these gives $D \sim (\bar{d}/\delta)^2 q$. If this relation were correct, then β_D in equation (10) should be 1. The discrepancy is likely due to the assumption that δ is constant in the flowing layer and averaging D across the entire flowing layer.

III. INFLUENCE OF CONTROL PARAMETERS ON PARTICLE SEGREGATION PATTERNS

Equations (8), (9), and (10) provide empirical relations that allow Λ and Pe to be written as functions of the control parameters q , L , d_s and d_l . Expressing q in terms of v_r (as previous experimental results indicate that v_r characterizes the transition from segregated to mixed states⁶) and noting that $d_s = 2\bar{d}/(d_l/d_s + 1)$, these equations yield

$$\begin{aligned} \Lambda &\propto \frac{\bar{d}^{0.05} L^{0.3} g^{0.35} \log(d_l/d_s)}{v_r^{0.7} d_l/d_s + 1}, \\ Pe &\propto \frac{\bar{d}^{0.055} v_r^{0.63}}{L^{0.37} g^{0.315}}, \end{aligned} \quad (11)$$

where g is the acceleration due to gravity. Because Λ and Pe are both weakly dependent on \bar{d} , similar segregation patterns are expected to occur at the same size ratio but different absolute particle sizes.

A. Comparison of model predictions to DEM simulations and experiments

To validate the theoretical model and the relations for the kinematic parameters derived in section II, the solution to equation (5) is compared to results from experiments⁶ and DEM simulations. In figure 7, the predicted particle concentration in the flowing layer (solution to equation (5)) is plotted for two different flow conditions. In each case the concentration of small particles is plotted as a function of position in the flowing

layer for both simulation (figure 7(a,b)) and theory (figure 7(c,d)) and at the bottom of the flowing layer (figure 7(e,f)), which represents concentration in the fixed bed. In both cases, the small particles percolate to the bottom of the flowing layer and deposit in the fixed bed (at $z = -\delta$) in the upstream region, while large particles rise to the top of the flowing layer, and are carried to the end of the flowing layer to deposit in the fixed bed in the downstream region. For $R = 1.5$ (left column), the grains remains better mixed compared to $R = 2$ (right column).

In figure 7(e-f), the small particle concentration at the bottom of the flowing layer is plotted as a function of the streamwise coordinate x as calculated from the theory, DEM simulation, and experiment. For both values of R , the theoretical predictions match well with both the DEM simulation and the experiment. The model slightly over-predicts the amount of segregation in the system, which is due to the approximation of the kinematic parameters by equations (8), (9), and (10). When the exact values of the kinematic parameters (measured from DEM simulations) are used, the theory predicts the segregation patterns even more accurately.¹³

B. Mixing and segregation

To quantify the degree of mixing in the flowing layer, we use the Danckwerts' intensity of segregation measure⁴⁹

$$I_d(c) = \frac{1}{\bar{c}(1-\bar{c})L} \int_0^L [c(x, -\delta) - \bar{c}]^2 dx, \quad (12)$$

where $\bar{c} = (1/L) \int_0^L c(x, -\delta) dx = 0.5$ is the spatially-averaged concentration at the bottom of the flowing layer. Note that I_d depends only on the concentration at the bottom of the flowing layer, as this is the concentration in the static bed. For a completely segregated final state, $I_d = 1$; for a completely mixed final state, $c = \bar{c}$ everywhere and $I_d = 0$.

To explore the dependence of I_d on the control parameters, I_d is plotted as a function of the rise velocity v_r for $L = 0.50$ m in figure 8 for four different mixtures with different R . The data points are determined from experiments,⁶ while the curve is obtained from theory using the relations in section II. For each set of mixtures in figure 8, I_d decreases as v_r increases since the particles move more quickly down the heap and have less time to segregate. Additionally, the best mixing (smallest I_d) occurs for the smallest R , while the strongest segregation (largest I_d) occurs for the largest R . For all the particle mixtures, the theoretical curve agrees qualitatively with the experimental data points, although the theory under-predicts the degree of mixing, as discussed in section III A. In spite of this, figure 8 demonstrates the power of the model together with equations (8)-(10) in

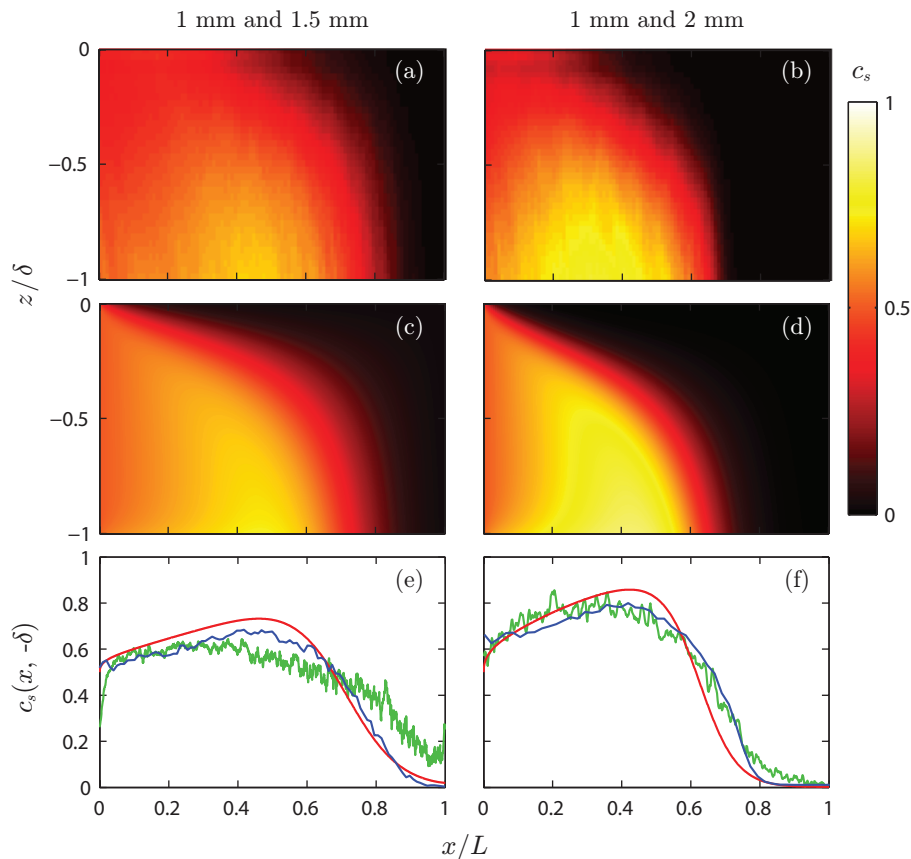


FIG. 7. Comparison of DEM simulations, experiments, and theoretical predictions (solutions of equation (5)) using the empirical relations for the kinematic parameters introduced in section II. Small particle concentration in the flowing layer measured from DEM simulations (a-b) and calculated from theory (c-d). (e-f) Small particle concentration at the bottom of the flowing layer ($z/\delta = -1$, bottom of panels (a-d)) for theory (dark grey, red online), simulation (black, blue online), and experiment (light grey, green online). (a,c,e) $d_s = 1$ mm, $d_l = 1.5$ mm, $L = 0.50$ m, $q = 1.2 \times 10^{-3}$ m²/sec. (b,d,f) $d_s = 1$ mm, $d_l = 2$ mm, $L = 0.50$ m, $q = 8.2 \times 10^{-4}$ m²/sec. Corresponding images of the experiment and the DEM simulation for (b,d,f) are shown in figure 2.

achieving reasonable predictions of the degree of segregation.

To demonstrate how the approach described here can be applied to practical granular segregation problems and to examine how the mixing metric varies in parameter space, figure 9 shows contours of constant I_d in (v_r, L) parameter space for $d_s = 1$ mm and $d_l = 2$ mm. The v_r and L values which correspond to points on any individual curve have the same value of I_d . Representative profiles of the small particle concentration in the flowing layer are shown for each value of I_d . From the contours, it is clear that if v_r increases, mixing increases. The degree of mixing is relatively insensitive to L so that v_r is the primary factor in determining the amount of segregation, similar to observations from experiments.⁶

It is possible to divide parameter space into regions of segregation and mixing. For any contour in figure 9, (v_r, L) values to the left of the curve result in a more segregated state, and values to the right result in a more mixed state. To explore particle segregation for different particle sizes, a threshold value of $I_d = 1/e$ is used to dis-

tinguish where the segregation changes in character from strong segregation to strong mixing, as is evident from the concentration profiles indicated in figure 9. In figure 10(a), curves of constant $I_d = 1/e$ are shown in (v_r, L) parameter space for different particle sizes. Each individual curve divides (v_r, L) parameter space into regions of mixed and segregated final states. For larger size ratios R , the curves shift to the right, decreasing the proportion of (v_r, L) parameter space that results in a mixed final state. For equal R (see three different $R = 2$ curves in figure 10(a)) but different \bar{d} , the curves are similar, since Λ and Pe depend only weakly on \bar{d} , as shown in equation (11).

In figure 10(b), curves of constant $I_d = 1/e$ are shown in (v_r, R) parameter space for $d_s = 1$ mm and different values of L . Values of v_r and R corresponding to the upper left of the figure result in a segregated final state; values of v_r and R corresponding to the lower right of the figure result in a mixed final state. As R approaches 1, the system is approximately monodisperse ($d_s \approx d_l$), and a mixed final state occurs for all v_r . Additionally, differ-

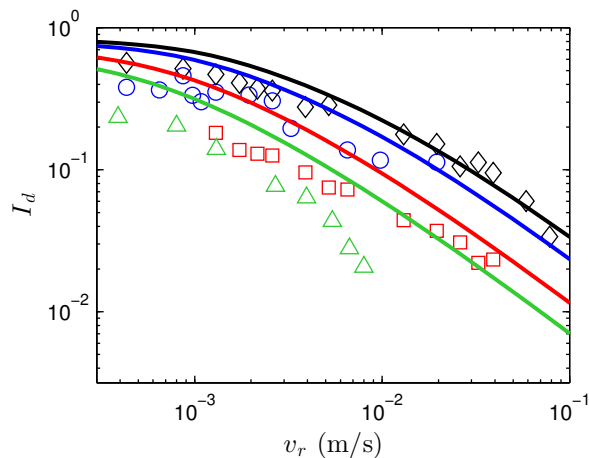


FIG. 8. Mixing (measured by I_d) vs. the rise velocity v_r for experiment (data points) and theory (curves). $d_s = 1$ mm, $d_l = 3$ mm, $R = 3$ (\diamond); $d_s = 1$ mm, $d_l = 2$ mm, $R = 2$ (\circ); $d_s = 1$ mm, $d_l = 1.5$ mm, $R = 1.5$ (\square); $d_s = 1.5$ mm, $d_l = 2$ mm, $R = 1.33$ (\triangle). $L = 0.50$ m.

ent values of L produce approximately the same curve of constant I_d , again implying that L does not have a large effect on the amount of mixing. Also, for $2 < R < 3$, the contours in figure 10(b) are not strongly dependent on R but depend more strongly on v_r . Therefore, $R = 2$ produces approximately the same amount of segregation as $R = 3$ for the same rise velocity, similar to observations from previous experiments.⁴⁰

To further validate the theoretical model, figure 11 shows experimental data points⁶ in (v_r, R) parameter space for $L = 1$ m. In the experiments, the metric $\Delta L/L = 0.15$ (which uses the length of the pure large particle region at the end of the flowing layer, ΔL) is used to determine the transition from mixing to segregation. To compare with theory, a curve of constant $I_d = 0.2$ is also shown in figure 11 for $L = 1$ m and $d_s = 1$ mm. The theoretical curve with $I_d = 0.2$ agrees well with the experimental data points (with a cut-off of $\Delta L/L = 0.15$), further supporting the validity of the theoretical model.

The important point here is that, with figure 10, it is possible to determine which dimensional control parameters in quasi-2D bounded heaps result in mixed final states and which result in segregated final states. In contrast, Fan *et al.*¹³ described how the final particle states depend on the two dimensionless parameters, Λ and Pe , which are functions of both control parameters and kinematic parameters, which require DEM simulations to determine.

IV. CONCLUSION

In this study, we have extended our previous work¹³ so that segregation patterns in size bidisperse quasi-2D bounded heaps can be determined solely from the sys-

tem control parameters (feed rate, flowing layer length, and particle diameters). In contrast, our previous work required values for the dimensionless parameters Λ and Pe , which depend on both the control parameters and the kinematic parameters, which must be measured from DEM simulations or experiments. Determining the relation of the control parameters to the kinematic parameters allows Λ and Pe to be calculated without the need for computationally costly DEM simulations. Thus one can determine which control parameter values result in segregated final states and which result in mixed final states. In addition, some of the scaling relations that are based on bounded heap flow, such as equation (8) for the percolation length scale, should be readily applicable to segregation in other granular flows such as rotating tumbler flow.²²

There is still much work to be done on theoretical modeling of granular mixing and segregation in bounded heaps. First, it is of substantial interest, particularly in industrial settings, to apply the segregation model to 3D bounded heaps, such as occur when filling a cylindrical silo, and preliminary results are promising.⁵⁰ Here, we considered only quasi-2D bounded heap flow, where the gap thickness was around 5 large particle diameters. Previous results⁵¹ indicate that gap thickness can play a role in the kinematics of the flow, and it is expected that varying T will change segregation patterns as well. In three-dimensional heaps, however, there is no gap thickness dependence.

Additionally, augmenting the model to describe a larger number of different particle sizes or even a continuous distribution of different particle sizes is an avenue that should be pursued. Finally, while this model was designed specifically for bounded heaps, the transport equation approach is likely applicable to other granular systems as well, including non-gravity driven flows. Generalizing the segregation model to these systems can potentially provide a universal framework for understanding the segregation and mixing of granular materials.

ACKNOWLEDGMENTS

This research was funded by NSF Grant CMMI-1000469 and The Dow Chemical Company. We thank Karl Jacob and Ben Freireich for helpful discussions of topics addressed in this paper.

¹O. Pouliquen, J. Delour, and S. B. Savage, “Fingering in granular flows,” *Nature*, vol. 386, pp. 816–817, 1997.

²H. A. Makse, S. Havlin, P. R. King, and H. E. Stanley, “Spontaneous stratification in granular mixtures,” *Nature*, vol. 386, pp. 379–382, 1997.

³J. M. Ottino and D. V. Khakhar, “Mixing and segregation of granular materials,” *Annu. Rev. Fluid Mech.*, vol. 32, pp. 55–91, 2000.

⁴I. S. Aranson and L. S. Tsimring, “Patterns and collective behavior in granular media: Theoretical concepts,” *Rev. Mod. Phys.*, vol. 78, pp. 641–692, 2006.

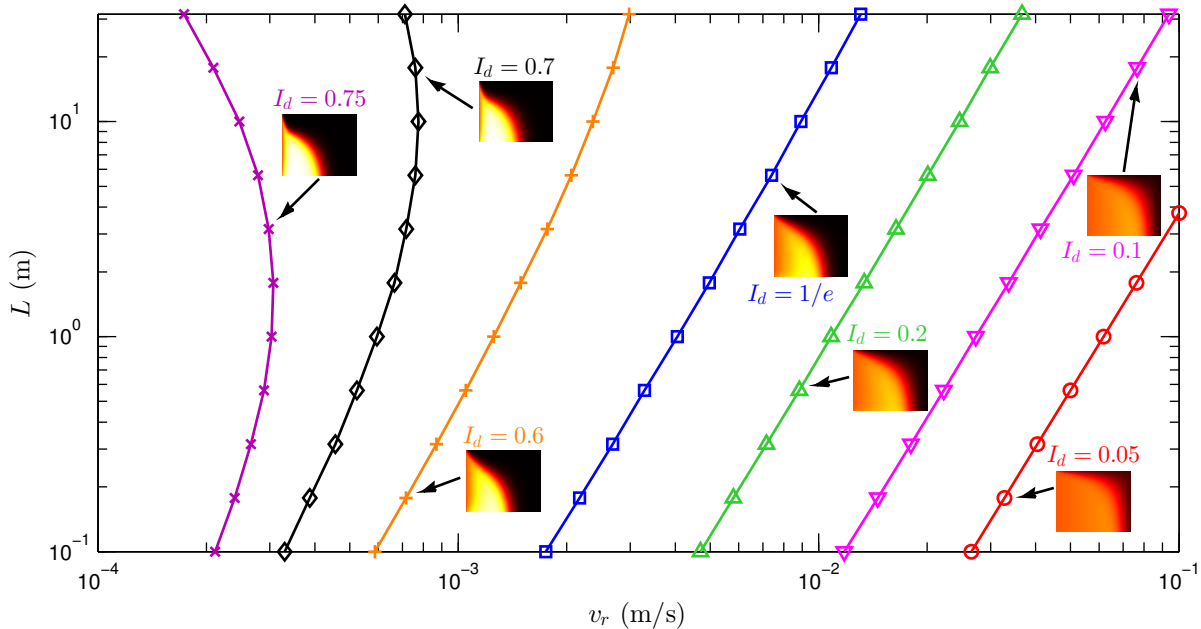


FIG. 9. Contours of constant mixing as measured by I_d in (v_r, L) parameter space for $d_s = 1$ mm, $d_l = 2$ mm, and different values of I_d . $I_d = 0.75$ (\times); $I_d = 0.7$ (\diamond); $I_d = 0.6$ ($+$); $I_d = 1/e$ (\square); $I_d = 0.2$ (\triangle); $I_d = 0.1$ (∇); $I_d = 0.05$ (\circ). Representative small particle concentration profiles are shown for each value of I_d .

- ⁵S. W. Meier, R. M. Lueptow, and J. M. Ottino, "A dynamical systems approach to mixing and segregation of granular materials in tumblers," *Adv. Phys.*, vol. 56, no. 5, pp. 757–827, 2007.
- ⁶Y. Fan, Y. Boukerkour, T. Blanc, P. B. Umbanhowar, J. M. Ottino, and R. M. Lueptow, "Stratification, segregation, and mixing of granular materials in quasi-two-dimensional bounded heaps," *Phys. Rev. E*, vol. 86, p. 051305, 2012.
- ⁷J. Bridgwater, "Mixing of powders and granular materials by mechanical means - a perspective," *Particuology*, vol. 10, no. 4, pp. 397–427, 2012.
- ⁸J. C. Williams, "The mixing of dry powders," *Powder Technol.*, vol. 2, pp. 13–20, 1968.
- ⁹J. A. Drahn and J. Bridgwater, "The mechanisms of free surface segregation," *Powder Technol.*, vol. 36, pp. 39–53, 1983.
- ¹⁰S. B. Savage and C. K. K. Lun, "Particle size segregation in inclined chute flow of dry cohesionless granular solids," *J. Fluid Mech.*, vol. 189, pp. 311–335, 1988.
- ¹¹K. M. Hill, D. V. Khakhar, J. F. Gilchrist, J. J. McCarthy, and J. M. Ottino, "Segregation-driven organization in chaotic granular flows," *Proc. Nat. Acad. Sci.*, vol. 96, pp. 11701–11706, 1999.
- ¹²S. E. Cisar, P. B. Umbanhowar, and J. M. Ottino, "Radial granular segregation under chaotic flow in two-dimensional tumblers," *Phys. Rev. E*, vol. 74, no. 5, p. 051301, 2006.
- ¹³Y. Fan, C. P. Schlick, P. B. Umbanhowar, J. M. Ottino, and R. M. Lueptow, "Modelling size segregation of granular materials: the roles of segregation, advection and diffusion," *J. Fluid Mech.*, vol. 741, pp. 252–279, 2014.
- ¹⁴H. Kruggel-Emden, E. Simsek, S. Rickelt, S. Wirtz, and V. Scherer, "Review and extension of normal force models for the Discrete Element Method," *Powder Technology*, vol. 171, pp. 157–173, Feb. 2007.
- ¹⁵G. Metcalfe, T. Shinbrot, J. J. McCarthy, and J. M. Ottino, "Avalanche mixing of granular solids," *Nature*, vol. 374, no. 6517, pp. 39–41, 1995.
- ¹⁶J. C. Williams, "The segregation of powders and granular materials," *Univ. Sheffield Fuel Soc. J.*, vol. 14, pp. 29–34, 1963.
- ¹⁷K. Shinohara, K. Shoji, and T. Tanaka, "Mechanism of size segregation of particles in filling a hopper," *Ind. Eng. Chem. Process Des. Dev.*, vol. 11, pp. 369–376, 1972.
- ¹⁸R. K. Goyal and M. S. Tomassone, "Power-law and exponential segregation in two-dimensional silos of granular mixtures," *Phys. Rev. E*, vol. 74, p. 051301, 2006.
- ¹⁹M. Rahman, K. Shinohara, H. Zhu, A. Yu, and P. Zulli, "Size segregation mechanism of binary particle mixture in forming a conical pile," *Chem. Eng. Sci.*, vol. 66, pp. 6089–6098, 2011.
- ²⁰T. Bouteux and P. de Gennes, "Surface flows of granular mixtures: I. general principles and minimal model," *J. Phys. I France*, vol. 6, pp. 1295–1304, 1996.
- ²¹T. Bouteux, "Surface flows of granular mixtures: II. segregation with grains of different size," *Eur. Phys. J. B*, vol. 6, no. 3, pp. 419–424, 1998.
- ²²C. P. Schlick, Y. Fan, P. B. Umbanhowar, J. M. Ottino, and R. M. Lueptow, "Segregation in rotating tumblers: Model implementation and scaling laws," *J. Fluid Mech.*, in review, 2014.
- ²³Y. Fan, P. B. Umbanhowar, J. M. Ottino, and R. M. Lueptow, "Kinematics of monodisperse and bidisperse granular flows in quasi-two-dimensional bounded heaps," *Proc. R. Soc. A*, vol. 469, p. 20130235, 2013.
- ²⁴J. M. N. T. Gray and V. A. Chugunov, "Particle-size segregation and diffusive remixing in shallow granular avalanches," *J. Fluid Mech.*, vol. 569, pp. 365–398, 2006.
- ²⁵J. M. N. T. Gray and A. R. Thornton, "A theory for particle size segregation in shallow granular free-surface flows," *Proc. R. Soc. A*, vol. 461, pp. 1447–1473, 2005.
- ²⁶J. M. N. T. Gray and C. Ancey, "Segregation, recirculation and deposition of coarse particles near two-dimensional avalanche fronts," *J. Fluid Mech.*, vol. 629, pp. 387–423, 2009.
- ²⁷B. Marks, P. Rognon, and I. Einav, "Grainsize dynamics of polydisperse granular segregation down inclined planes," *J. Fluid Mech.*, vol. 690, pp. 499–511, 2011.
- ²⁸S. Wiederseiner, N. Andreini, G. Epely-Chauvin, G. Moser, M. Monnerieu, J. M. N. T. Gray, and C. Ancey, "Experimental investigation into segregating granular flows down chutes," *Phys. Fluids*, vol. 23, p. 013301, 2011.
- ²⁹Y. Fan and K. M. Hill, "Theory for shear-induced segregation of dense granular mixtures," *New J. Phys.*, vol. 13, p. 095009, 2011.

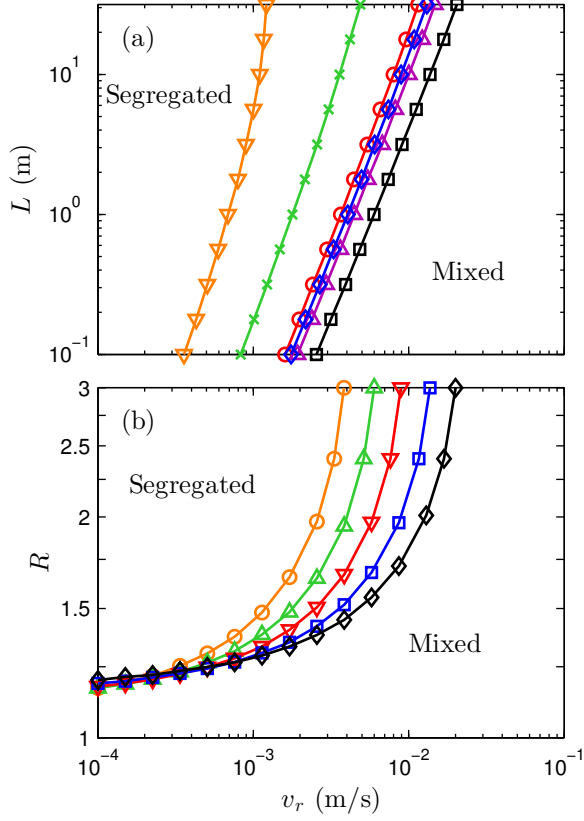


FIG. 10. Contours of constant mixing ($I_d = 1/e$), showing regions of parameter space that yield mixed and segregated states. (a) (v_r, L) parameter space for different particle sizes: $d_s = 1$ mm, $d_l = 1.3$ mm (∇); $d_s = 1$ mm, $d_l = 1.5$ mm (\times); $d_s = 1$ mm, $d_l = 2$ mm (\diamond); $d_s = 1$ mm, $d_l = 3$ mm (\square); $d_s = 0.5$ mm, $d_l = 1$ mm (\circ); $d_s = 2$ mm, $d_l = 4$ mm (\triangle). (b) (v_r, R) parameter space for $d_s = 1$ mm and different L : $L = 0.3$ m (\circ); $L = 1$ m (\triangle); $L = 3$ m (∇); $L = 10$ m (\square); $L = 30$ m (\diamond).

- ³⁰A. Thornton, T. Weinhart, S. Luding, and O. Bokhove, "Modeling of particle size segregation: Calibration using the discrete particle method," *Int. J. Mod. Phys. C*, vol. 23, no. 08, p. 1240014, 2012.
- ³¹D. R. Tunuguntla, O. Bokhove, and A. R. Thornton, "A mixture theory for size and density segregation in shallow granular free-surface flows," *J. Fluid Mech.*, vol. 749, pp. 99–112, 2014.
- ³²L. B. H. May, L. A. Golick, K. C. Phillips, M. Shearer, and K. E. Daniels, "Shear-driven size segregation of granular materials: Modeling and experiment," *Phys. Rev. E*, vol. 81, p. 051301, 2010.
- ³³P. Chen, J. M. Ottino, and R. M. Lueptow, "Granular axial band formation in rotating tumblers: a discrete element method study," *New J. Phys.*, vol. 13, p. 055021, 2011.
- ³⁴L. E. Silbert, G. S. Grest, R. Brewster, and A. J. Levine, "Rheology and contact lifetimes in dense granular flows," *Phys. Rev. Lett.*, vol. 99, p. 068002, 2007.
- ³⁵The separate streamwise velocity profiles for large and small particles were measured from DEM simulations and compared. The assumption that they are the same was found to be valid throughout most of the streamwise direction.
- ³⁶While k can be chosen such that the surface velocity approaches a smaller fraction of the surface velocity, DEM simulations indicate that the concentration changes minimally in the normal direction

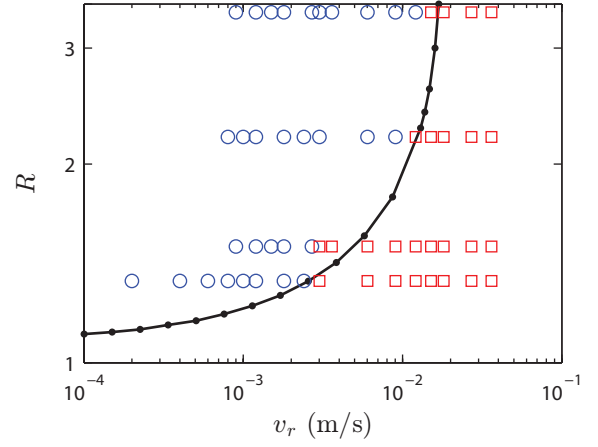


FIG. 11. (v_r, R) parameter space for $d_s = 1$ mm and $L = 1$ m showing regions of mixing and segregation. The curve represents the constant mixing contour with $I_d = 0.2$ calculated from theory. The data points are from experiments⁶ using the metric $\Delta L/L = 0.15$, yielding segregated (\circ) and mixed (\square) final states.

below this cut-off.

- ³⁷V. N. Dolgunin, A. N. Kudy, and A. A. Ukolov, "Development of the model of segregation of particles undergoing granular flow down an inclined chute," *Powder technol.*, vol. 96, no. 3, pp. 211–218, 1998.
- ³⁸S. K. Hajra, D. Shi, and J. J. McCarthy, "Granular mixing and segregation in zigzag chute flow," *Phys. Rev. E*, vol. 86, 2012.
- ³⁹For the example in figure 4, there are no regions in the flowing layer where $c_s > 0.7$. Therefore, there is no data for the percolation velocity for $(1 - c_l) > 0.7$ and $(1 - c_s) < 0.3$.
- ⁴⁰L. A. Golick and K. E. Daniels, "Mixing and segregation rates in sheared granular materials," *Phys. Rev. E*, vol. 80, no. 4, 2009.
- ⁴¹Y. Tsuji, T. Tanaka, and T. Ishida, "Lagrangian numerical simulation of plug flow of cohesionless particles in a horizontal pipe," *Powder Technol.*, vol. 71, pp. 239–250, 1992.
- ⁴²B. K. Mishra and C. V. R. Murty, "On the determination of contact parameters for realistic DEM simulations of ball mills," *Powder Technol.*, pp. 290–297, 2001.
- ⁴³T. Brosh, H. Kalman, and A. Levy, "Accelerating CFDDEM simulation of processes with wide particle size distributions," *Particology*, vol. 12, pp. 113–121, 2014.
- ⁴⁴B. Utter and R. P. Behringer, "Self-diffusion in dense granular shear flows," *Phys. Rev. E*, vol. 69, p. 031308, 2004.
- ⁴⁵J. Bridgwater, "Self-diffusion coefficients in deforming powders," *Powder Technol.*, vol. 25, no. 1, pp. 129–131, 1980.
- ⁴⁶C. S. Campbell, "Self-diffusion in granular shear flows," *J. Fluid Mech.*, vol. 348, no. 1, pp. 85–101, 1997.
- ⁴⁷S. B. Savage and R. Dai, "Studies of granular shear flows wall slip velocities, layering and self-diffusion," *Mech. Mater.*, vol. 16, no. 1, pp. 225–238, 1993.
- ⁴⁸Y. Fan, P. B. Umbanhowar, J. M. Ottino, and R. M. Lueptow, "Shear-rate-independent collisional diffusion in granular materials: from rapid to creep flow," *Phys. Rev. Lett.*, *In preparation*.
- ⁴⁹P. V. Danckwerts, "The definition and measurement of some characteristics of mixtures," *Appl. Sci. Res. A*, vol. 3, no. 4, pp. 279–296, 1952.
- ⁵⁰C. P. Schlick, *Applications of advection-diffusion based methodologies to fluid and granular flows*. PhD thesis, Northwestern University, 2014.
- ⁵¹P. Jop, Y. Forterre, and O. Pouliquen, "Crucial role of sidewalls in granular surface flows: consequences for the rheology," *J. Fluid Mech.*, vol. 541, pp. 167–192, 2005.

- ⁵²I. C. Christov, J. M. Ottino, and R. M. Lueptow, “From streamline jumping to strange eigenmodes: Bridging the lagrangian and eulerian pictures of the kinematics of mixing in granular flows,” *Phys. Fluids*, vol. 23, no. 10, p. 103302, 2011.
- ⁵³C. P. Schlick, I. C. Christov, P. B. Umbanhowar, J. M. Ottino, and R. M. Lueptow, “A mapping method for distributive mixing with diffusion: Interplay between chaos and diffusion in time-periodic sine flow,” *Phys. Fluids*, vol. 25, no. 5, 2013.
- ⁵⁴M. K. Singh, O. S. Galaktionov, H. E. H. Meijer, and P. D. Anderson, “A simplified approach to compute distribution matrices for the mapping method,” *Comput. Chem. Eng.*, vol. 33, no. 8, pp. 1354–1362, 2009.

Appendix A: Numerical method and boundary conditions

Boundary conditions are required to solve equation (5). At the flow inlet, $\tilde{x} = 0$, the particles are well-mixed, so $c_s(0, \tilde{z}) = c_l(0, \tilde{z}) = 0.5$. At the right end of the heap ($\tilde{x} = 1$), the flow is parallel to the boundary and diffusion and segregation only act in the normal direction, so no boundary condition is needed. At the bottom and top of the flowing layer ($\tilde{z} = -1, 0$), the segregation flux is equal

to the diffusion flux, as in in Gray and Chugunov,²⁴ so

$$\Lambda h(\tilde{x}, \tilde{z}) c_i (1 - c_i) = \frac{1}{\text{Pe}} \frac{\partial c_i}{\partial \tilde{x}}. \quad (\text{A1})$$

The boundary condition at the bottom of the flowing layer implies that particles do not leave the heap due to diffusion and segregation, but to advection alone at a velocity equal to the rise velocity of the heap. For details of the validity of this boundary condition for bounded heaps, see Fan *et al.*¹³

Equation (5) is solved with an operator splitting scheme,^{52,53} so the advection and segregation/diffusion steps are solved separately. The advection step is solved with a matrix mapping method,⁵⁴ and the segregation/diffusion step is solved using the implicit Crank-Nicolson method. This method is efficient because, in steady state, the concentration along a vertical line through the domain (constant $\tilde{x} = \tilde{x}_0$, $-1 < \tilde{z} < 0$) depends only on the upstream concentration ($\tilde{x} < \tilde{x}_0$). Therefore, the concentration in steady state can be solved sequentially, starting at the inlet $\tilde{x} = 0$ and progressing toward the end wall at $\tilde{x} = 1$. Further details concerning the numerical method can be found in Fan *et al.*¹³